A Dos-Enhanced Numerical Simulation of Heat Transfer and Fluid Flow Through an Array of Offset Fins With Conjugate Heating in the Bounding Solid

Ephraim M. Sparrow
Mechanical Engineering Department,
University of Minnesota,
Minneapolis, MN

John P. Abraham
e-mail address: jpabraham@stthomas.edu
Department of Engineering,
University of St. Thomas,
St. Paul, MN

Paul W. Chevalier
Mechanical Engineering Department,
University of Minnesota,
Minneapolis, MN

The method of Design of Simulation (DOS) was used to guide and enhance a numerical simulation of fluid flow and heat transfer through offset-fin arrays which form the interior geometry of a cold plate. The basic problem involved 11 independent parameters. This prohibitive parametric burden was lessened by the creative use of nondimensionalization that was brought to fruition by a special transformation of the boundary conditions. Subsequent to the reduction of the number of parameters, the DOS method was employed to limit the number of simulation runs while maintaining an accurate representation of the parameter space. The DOS method also provided excellent correlations of both the dimensionless heat transfer and pressure drop results. The results were evaluated with respect to the Colburn Analogy for heat and momentum transfer. It was found that the offseting of the fins created a larger increase in the friction factor than that which was realized for the dimensionless heat transfer coefficient. [DOI: 10.1115/1.1800531]

Introduction

The use of cold plates as a means for cooling electronic equipment is a well-established technology. However, in response to the ever-increasing heat loads that must be dealt with, the geometric complexity of cold plates has increased markedly in recent years. For example, in a very recent application involving the cooling of magnetrons for radar applications, a cold-plate configuration has been proposed in which the passages for the coolant consist of five highly distinctive geometries in series, each with its own particular complexity. Although, in principle, experiments can be undertaken for specific cold-plate geometries, this approach is not cost-effective during a development process in which optimal geometrical passage configurations are being sought [1–10].

To facilitate an evaluation of the characteristics of various candidate cold-plate geometries, effective use may be made of numerical simulations. Although this approach is, in principle, well suited for the identification of optimal configurations, it, too, has potential operational drawbacks. For instance, an appraisal of the number of independent parameters which describe the geometrical and operating conditions may well reveal a dozen or more. As a consequence, a more efficient approach that goes beyond mere numerical simulation must be employed.

In the present investigation, where a highly complex, three-dimensional flow passage is to be considered, there are a total of 11 independent geometrical and operating parameters. This prohibitive parametric load has to be reduced to a more reasonable set before simulation can be considered. Two techniques were employed to diminish the number of parametric inputs. One of these is skillful use of nondimensionalization. The other technique is akin to the well-established method used in experimental work to extract the maximum amount of information from the minimum number of data runs. That technique is commonly known as ''Design of Experiments'' (DOE) [11]. In what follows, the method to be used here for the selection of simulation runs will be denoted as ''Design of Simulations'' (DOS).

Contributed by the Heat Transfer Division for publication in the JOURNAL OF HEAT TRANSFER. Manuscript received by the Heat Transfer Division April 12, 2004; revision received July 10, 2004. Assoc. Editor: C. Amon.

The specific cold-plate configuration to be considered here is an array of offset fins contained between two large cover plates. The array is made up of a large number of rows such that it is expected that sufficiently far downstream from the array inlet, a periodic flow pattern will develop. This type of flow pattern is called periodically fully developed by Patankar, Sparrow, and Liu [12]. There is, however, a hydrodynamic development region which must be dealt with in the numerical simulation. With regard to heat transfer, it is expected that there will also exist a thermally developed regime in which the heat transfer coefficient for each module of the array becomes a constant. Here again, there is a region immediately downstream of the inlet in which the temperature field develops.

The goals of the research encompass both heat transfer and pressure drop. From the standpoint of engineering practice, emphasis will be placed on identifying those geometrical and operating parameters which have the greatest impact on the aforementioned results. The identification of the relative importance of the parameters will be enabled by the DOS method. In addition to the identification of the importance of the various parameters, the DOS method will provide quantitative algebraic relationships for the dimensionless heat transfer coefficient (the Stanton number) and the dimensionless pressure gradient (friction factor). The determination of Stanton numbers and friction numbers enables the evaluation of the Colburn Analogy (a modification of the Reynolds Analogy). The nature of the flow field development will be exhibited by means of contour diagrams.

The numerical simulations were performed by means of ANSYS FLOTRAN software. This is a finite-element-based program that is one of the suite of programs of the ANSYS package.

Minimization of Parametric Inputs. From an examination of the governing differential equations and boundary conditions, 11 parameters were identified. These included (a) physical dimensions: interfin spacing, fin length, fin thickness, and fin height; (b) boundary conditions: surface heat flux, fluid inlet temperature, and inlet fluid velocity; and (c) thermophysical properties: fin conductivity, fluid conductivity, fluid specific heat, and fluid density. The first task of the analysis is to reduce the number of parametric

inputs to a manageable value. Two methods will be used to accomplish this goal. These tasks will be set forth in the order in which they were employed.

Nondimensionalization of the Governing Equations. The starting point of the nondimensionalization is the governing conservation equations and the appropriate boundary conditions. The nondimensionalization proceeds rather smoothly for the governing equations, but special care has to be taken when the boundary conditions are made dimensionless. Since the problem is three dimensional, there are five governing equations: three momentum conservation equations, the energy equation, and the mass conservation equation. Since the nondimensionalization of the momentum equations is similar for all three, it is necessary for present purposes to work with only one of them. For concreteness, the *x*-direction momentum equation will be considered. For laminar, constant property fluid flow, the *x*-momentum equation is:

$$\rho\left(u\frac{\partial u}{\partial x}+v\frac{\partial u}{\partial y}+w\frac{\partial u}{\partial z}\right)=-\frac{\partial p}{\partial x}+\mu\left(\frac{\partial^2 u}{\partial x^2}+\frac{\partial^2 u}{\partial y^2}+\frac{\partial^2 u}{\partial z^2}\right) \quad (1)$$

The relevant energy and mass conservation equations are

$$\rho c_p\left(u\frac{\partial t}{\partial x}+v\frac{\partial t}{\partial y}+w\frac{\partial t}{\partial z}\right)=k_{\text{fluid}}\left(\frac{\partial^2 t}{\partial x^2}+\frac{\partial^2 t}{\partial y^2}+\frac{\partial^2 t}{\partial z^2}\right) \quad (2)$$

$$\frac{\partial u}{\partial x}+\frac{\partial v}{\partial y}+\frac{\partial w}{\partial z}=0 \quad (3)$$

The next step is to select reference quantities to serve as the basis for the nondimensionalization. Natural reference quantities include (a) the mean velocity of the flow $\overline{U}$ and (b) one of the characteristic dimensions of the system. The chosen reference dimension is the width ω of a flow passage in the fin array. For the temperature *t*, it is appropriate both to shift the datum and to scale the magnitude. With regard to scaling the magnitude of the dimensionless temperature, cognizance has to be taken of the nature of the thermal boundary conditions. For the present problem, the thermal boundary conditions are a given inlet temperature ($t=t_0$) for the fluid flow and uniform heat flux q_{surf} at the bounding walls of the cold plate. When these conditions are taken into account, it is natural to use t_0 as the datum and the reference temperature as $q_{\text{surf}}\omega/k_{\text{fluid}}$. By the use of these reference quantities, the dimensions, coordinates, velocities, and temperature emerge in dimensionless form as

$$\tau=T/\omega, \quad \lambda=L/\omega, \quad \eta=H/\omega \quad (4)$$

$$X=x/\omega, \quad T=y/\omega, \quad Z=z/\omega \quad (5)$$

$$U=u/\overline{U}, \quad V=v/\overline{U}, \quad W=w/\overline{U} \quad (6)$$

$$\Theta=\frac{t-t_0}{(q_{\text{surf}}\omega/k_{\text{fluid}})} \quad (7)$$

In these equations, the quantities *T*, *L*, *H*, and ω represent the dimensions of the offset fin array. To provide perspective for these quantities, it is useful to make reference to Fig. 1. The figure is a schematic diagram of a representative subsection of the array. In this figure, the fins are portrayed as the darker-shaded regions and are further identified by a callout. The space between the fins is the region of fluid flow. Further inspection of the figure shows that there are two degrees of periodicity. In the flow direction, the geometry repeats with a period of 2L while in the transverse direction, the periodic length is $\omega+T$.

Also indicated in the figure is the thermal boundary condition that has been imposed on the upper cover plate of the array. Although not shown in the diagram, the lower cover plate of the array is also a surface of uniform heat flux of the same magnitude as that of the upper cover plate. Consequently, there is a plane of thermal symmetry situated midway between the upper and lower cover plates. This plane of symmetry also corresponds to a plane

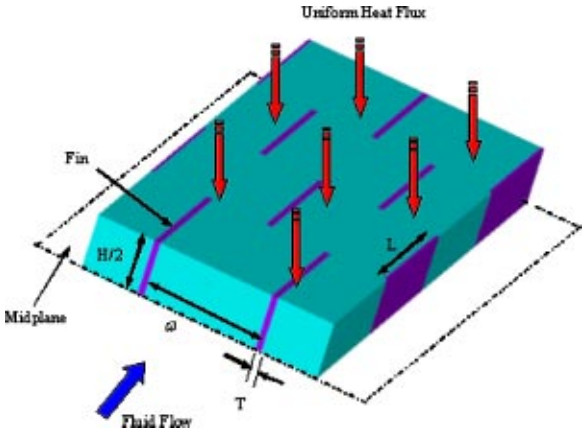

Fig. 1 Schematic diagram of a representative subsection of the offset fin array

of symmetry for fluid flow. This symmetry plane has been designated as the midplane and is indicated as such in the figure. Further inspection of the figure indicates that L is the length of an individual fin in the flow direction, ω is the transverse inter-fin spacing, *T* is the thickness of the material from which the fins are made, and *H* is the total channel height between the cover plates.

Attention may be redirected to the nondimensionalization process. It still remains to make the pressure into a dimensionless quantity, and the suitable reference quantity is $\rho\overline{U}^2$, so that

$$P=\frac{P}{\rho\overline{U}^2} \quad (8)$$

When the dimensionless variables and parameters defined in Eqs. (4)–(8) are inserted into the conservation equations, Eqs. (1)–(3), additional dimensionless groups emerge. They are,

$$\text{Re}=\frac{\rho\omega\overline{U}}{\mu}$$

$$\text{Pe}=\frac{\rho c_P\omega\overline{U}}{k_{\text{fluid}}}=\text{Re}\cdot\text{Pr} \quad (9)$$

$$\text{Pr}=\frac{c_P\mu}{k_{\text{fluid}}}$$

With these, Eqs. (1)–(3) become

$$U\frac{\partial U}{\partial X}+V\frac{\partial U}{\partial Y}+W\frac{\partial U}{\partial Z}=-\frac{\partial P}{\partial X}+\frac{1}{\text{Re}}\left(\frac{\partial^2 U}{\partial X^2}+\frac{\partial^2 U}{\partial Y^2}+\frac{\partial^2 U}{\partial Z^2}\right) \quad (10)$$

$$U\frac{\partial\Theta}{\partial X}+V\frac{\partial\Theta}{\partial Y}+W\frac{\partial\Theta}{\partial Z}=\frac{1}{\text{Pe}}\left(\frac{\partial^2\Theta}{\partial X^2}+\frac{\partial^2\Theta}{\partial Y^2}+\frac{\partial^2\Theta}{\partial Z^2}\right) \quad (11)$$

$$\frac{\partial U}{\partial X}+\frac{\partial V}{\partial Y}+\frac{\partial W}{\partial Z}=0 \quad (12)$$

When these equations are to be modeled in FLOTRAN, note must be taken that the software is configured to work with dimensional quantities. In fact, the software works with Eqs. (1)–(3). To facilitate using the software as written, it is appropriate to introduce values of density, specific heat, viscosity, and thermal conductivity which brings congruence between Eqs. (1)–(3) and Eqs. (10)–(12). A comparison of these equations yields

$$\rho=1, \quad c_p=1,$$
$$\mu=1/\text{Re}, \quad k_{\text{fluid}}=1/\text{Pe} \quad (13)$$

These nondimensional thermophysical properties are, of course, different from the actual thermophysical properties. They will be termed pseudo properties. To make this distinction, a superscript ($'$) is appended to each of the pseudo properties so that

$$\rho' = 1, \quad c_p' = 1, \qquad \mu' = 1/\mathrm{Re}, \quad k'_{\mathrm{fluid}} = 1/\mathrm{Pe} \tag{14}$$

Nondimensionalization and Transformation of the Boundary Conditions. The nondimensionalization of the governing differential equations is now complete. Next, consideration will be given to the boundary conditions and the continuity conditions at internal solid-fluid interfaces. It is convenient to deal first with the continuity conditions. The continuity of temperature is automatically satisfied by the nature of the computer program. On the other hand, for heat flux continuity,

$$\left(k\frac{\partial T}{\partial n}\right)_{\mathrm{fluid}} = \left(k\frac{\partial T}{\partial n}\right)_{\mathrm{solid}} \tag{15}$$

where n represents the normal to the interface in question. The insertion of the dimensionless parameters and variables leads to

$$\left(k\frac{\partial \Theta}{\partial N}\right)_{\mathrm{fluid}} = \left(k\frac{\partial \Theta}{\partial N}\right)_{\mathrm{solid}} \tag{16}$$

where $N = n/\omega$. As was set forth in connection with Eq. (14), the computer program was operated with pseudo properties in lieu of the actual thermophysical properties. Therefore, as far as the software is concerned, the value of k_{fluid} is $k'_{\mathrm{fluid}} = 1/\mathrm{Pe}$. Correspondingly, the operational value of k_{solid} must also be a pseudo property k'_{solid}. Therefore, from Eq. (16), it is seen that to preserve heat flux continuity at a solid-fluid interface

$$\frac{k'_{\mathrm{solid}}}{k'_{\mathrm{fluid}}} = \frac{k_{\mathrm{solid}}}{k_{\mathrm{fluid}}} \tag{17}$$

which leads to

$$k'_{\mathrm{solid}} = \frac{1}{\mathrm{Pe}}\left(\frac{k_{\mathrm{solid}}}{k_{\mathrm{fluid}}}\right) \tag{18}$$

The value of the pseudo conductivity k'_{solid} given in Eq. (18) was used as an input to the software.

The heat flux condition on the cover plates will now be assessed. In applying the given heat flux boundary condition, it is noted that the thicknesses of the respective cover plates were set at a very small value (infinitesimally thin) in order to avoid the occurrence of an additional parameter. A physical consequence of this assumption is that there is no spreading of heat in the plane of a cover plate. Another consequence is that the applied heat flux is imposed directly on the flowing fluid or the base of a fin.

For the case in which the heat flux is applied directly to the flowing fluid, the application of the given heat flux boundary condition yields

$$q_{\mathrm{surf}} = k_{\mathrm{fluid}}(\partial T/\partial n)_{\mathrm{fluid}} \tag{19}$$

in which n is the outward normal on the top cover plate. When the nondimensional variables and parameters are introduced into this equation, there follows:

$$(\partial \Theta/\partial N)_{\mathrm{fluid}} = 1 \tag{20}$$

Although this equation is correct, it does not provide information that is acceptable for the software. In fact, the software requires the input of a value of the heat flux itself rather than the temperature gradient. When the software is operated using the dimensionless temperature gradient $\partial\Theta/\partial N$ and the pseudoproperty k'_{fluid}, the heat flux boundary condition at the cover plate becomes

$$q'_{\mathrm{surf}} = k'_{\mathrm{fluid}}(\partial \Theta/\partial N)_{\mathrm{fluid}} \tag{21}$$

The derivative is given by Eq. (20), and k'_{fluid} is expressed by Eq. (14), so that

$$q'_{\mathrm{surf}} = 1/\mathrm{Pe} \tag{22}$$

For the case in which the heat flux is applied to the portion of the cover plate which mates with a fin,

$$q_{\mathrm{surf}} = \left(k\frac{\partial T}{\partial n}\right)_{\mathrm{solid}} \tag{23}$$

When this equation is transformed into the variables of the analysis, it is found that

$$q'_{\mathrm{surf}} = 1/\mathrm{Pe} \tag{24}$$

From the foregoing development, it is seen that the heat flux to be provided to the FLOTRAN software is 1/Pe.

For the temperature problem, it remains to specify the boundary conditions at the inlet and at a location far downstream from the inlet. Since $t = t_0$ at the inlet, then, Eq. (7) gives

$$\Theta_{\mathrm{inlet}} = 0 \tag{25}$$

Far downstream from the inlet, the standard outflow boundary conditions are imposed.

$$\partial \Theta/\partial X = 0 \tag{26}$$

Attention will now be turned to the boundary conditions for the velocity problem. The software automatically enforces the no-slip condition at all solid-fluid interfaces, and this condition continues in force for the dimensionless velocities. At the inlet to the array, the streamwise velocity in dimensionless form becomes

$$U = 1 \tag{27}$$

and the other velocity components are zero. At a far downstream location, the standard outflow boundary conditions were applied.

It is appropriate to assess what has thus far been accomplished in the task of parameter reduction. At this stage of the task, there remain five dimensionless parameters: Re, Pe, $k_{\mathrm{solid}}/k_{\mathrm{fluid}}$, τ (fin thickness), λ (fin length), and η (fin height). In the forthcoming numerical calculations, specific consideration will be given to air as the coolant fluid. This selection fixes Pr and, thereby, eliminates Pe ($=\mathrm{Re}\,\mathrm{Pr}$) as a separate parameter. In addition, in view of current practice, the fin height parameter η was set equal to 1.0. Therefore, at this stage of the analysis, the numerical simulations require the specification of four parameters.

Design of Simulations (DOS). To initiate the implementation of the DOS approach, the first step is to select high and low values of the four parameters. This selection provides eight numerical values which may be identified as $\mathrm{Re}_{\mathrm{hi}}$, $\mathrm{Re}_{\mathrm{lo}}$, τ_{hi}, ... By making use of the selected values, a table is formed which will be used as the basis of the simulation runs. As can be seen from Table 1, 16 cases have been synthesized using permutations and combinations of the aforementioned hi and lo values of the parameters.

Execution of the Simulations

The FLOTRAN finite-element software was utilized to perform the numerical simulations. This program is one of the suite of programs of the ANSYS package. The simulations were run using approximately 15,000 elements, and each of the 16 cases required approximately 200 iterations to achieve convergence. The elements chosen to span the solution domain were strictly quadrilateral. From the menu of available solvers, the SIMPLEF pressure-velocity coupling was selected, which is an enhanced version of the well-established SIMPLE velocity-pressure coupling technique. For the solution of the simultaneous equations which are inherent in the simulation, the following solvers were selected, on the basis of advice provided in the ANSYS operation manual: (a)

Table 1 DOS parameter list

Case	Re	k_{solid}/k_{fluid}	τ	λ
1	100 (lo)	646 (lo)	0.05 (lo)	1.0 (lo)
2	2000 (hi)	646	0.05	1.0
3	100	6460 (hi)	0.05	1.0
4	2000	6460	0.05	1.0
5	100	646	0.10 (hi)	1.0
6	2000	646	0.10	1.0
7	100	6460	0.10	1.0
8	2000	6460	0.10	2.0 (hi)
9	100	646	0.05	2.0
10	2000	646	0.05	2.0
11	100	6460	0.05	2.0
12	2000	6460	0.05	2.0
13	100	646	0.10	2.0
14	2000	646	0.10	2.0
15	100	6460	0.10	2.0
16	2000	6460	0.10	2.0

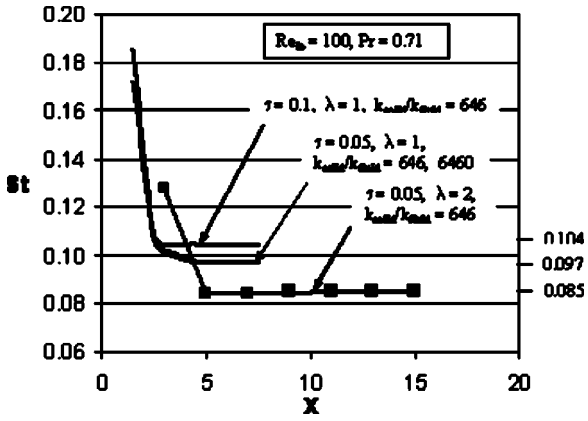

Fig. 2 Per-module Stanton numbers for $Re_{lo}=100$

for the velocity field, the TriDiagonal Matrix Algorithm (TDMA); (b) for the pressure field, the Preconditioned Conjugate Gradient; and (c) for the temperature, the Preconditioned Generalized Minimum Residual Method.

Since the solution domain is, in principle, doubly infinite, steps were taken to reduce it to manageable size while maintaining all of the essential physical features of the fin array. Since the geometry forces the attainment of periodically fully developed flow in the streamwise direction, it was only necessary to extend the solution domain through the hydrodynamic entrance region. The thermal boundary conditions also are conducive to the attainment of a thermally developed situation, so that, once again, the thermal entrance region was all that had to be traversed. The transverse width of the solution domain was bounded by the use of symmetry lines. Advantage was also taken of the existence of the symmetry plan midway between the upper and lower coverplates (see Fig. 1 where the midplane is identified).

Results and Discussion

The presentation of the results will include four different foci that, in the order of appearance, are (1) quantitative heat transfer and pressure drop results, (2) Colburn Analogy connecting heat transfer and pressure drop, (3) correlation of the results by means of the DOS method, and (4) flow-field and pressure-field contour diagrams.

Quantitative Heat Transfer Results. The results of greatest interest include the heat transfer and pressure drop characteristics of the offset fin array. For both the heat transfer and the pressure drop, results will be presented for the entrance region values, the periodically fully developed values, and the length of the entrance region. The presentation begins with a graphical depiction of local heat transfer and pressure distributions. For the case of heat transfer, the presented results are for a module-averaged heat transfer coefficient $\bar{h}$ which, in dimensionless form, is represented by the per-module Stanton number, $St=\bar{h}/(\rho c_p U)$. The numerical results for the Stanton number are presented in Figs. 2 and 3.

The streamwise distribution of the per-module Stanton number for the low Reynolds number Re_{lo} are set forth in Fig. 2 for various parametric values of the dimensions and conductivity ratio. As can be seen from the figure, the Stanton number decreases sharply through the thermal entrance region and achieves a fully developed value. In particular, the fully developed state is attained at $x/\omega \approx 3-4$ for the cases depicted in the figure. This result is surprisingly close to what would be predicted from laminar, pipe-flow theory, which gives the entrance length as approximately 0.05 Re Pr. For instance, for Re=100 and Pr=0.71, the pipe-flow entrance length would be approximately 3.5 diameters!

Perspective on the magnitude of the Stanton numbers can be obtained by considering fully developed, laminar heat transfer in a square duct for which the fully developed Nusselt number is 3.6. The square duct is chosen for a comparison case because the present offset-fin geometry has cross-sectional shape which is square (fin height=interfin spacing). From the definition of the Stanton number, St=Nu/Pe, the fully developed Stanton number for the square duct is 3.6/71=0.051. This value is to be compared with the fully developed Stanton numbers that are indicated at the right-hand margin of Fig. 2. Those values are substantially higher than 0.051, which is for fully developed duct flow. This difference is fully accounted when consideration is given to the differences between the cases being compared. Of greatest significance is the fact that in the fully developed regime for the offset fins, new boundary layers are periodically initiated at the beginning of each module. The boundary layer development is responsible for the enhanced heat transfer coefficients.

As a final discussion item with respect to Fig. 2, the physical basis of the vertical arrangement of the curves will now be addressed. The effect of fin thermal conductivity is clearly of no importance. The fin-thickness effect is slight but is not totally negligible as witnessed by the spread between the two uppermost curves in the figure. Of somewhat greater significance, but still not of major importance, is the effect of fin length. The greater fin length enables a thicker boundary layer to grow in the streamwise direction and, as a consequence, the per-module heat transfer coefficient must decrease. As a closure to Fig. 2, attention may be called to the local minimum in the lowermost curve.

Results similar to those of Fig. 2, but for $Re_{hi}=2000$, are presented in Fig. 3. Inspection of Fig. 3 and comparison with Fig. 2 reveals a significant difference in the values of the Stanton number as witnessed by the differing ordinate scales. Most of the difference between the two sets of Stanton numbers is actually inherent in the definition of the quantity itself. This is readily seen by noting that the heat transfer coefficient in the Stanton number

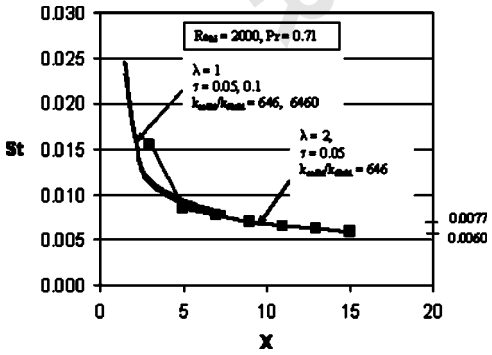

Fig. 3 Per-module Stanton numbers for $Re_{hi}=2000$

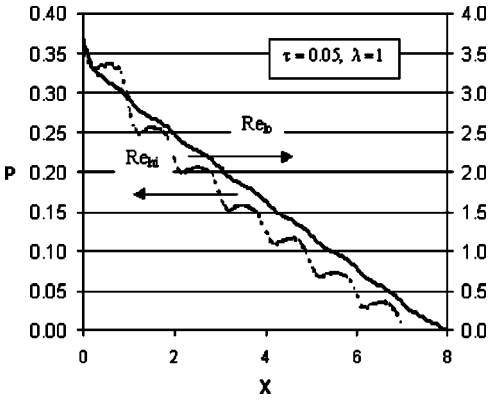

Fig. 4 Variation of the dimensionless pressure with streamwise position along the midplane of the array, $\tau=0.05$, $\lambda=1$

is divided by the mean velocity. Since the higher Reynolds number corresponds to a higher velocity, it is reasonable that smaller Stanton numbers correspond to higher Reynolds numbers. In this regard, it is also of interest to compare the fully developed Stanton numbers of Fig. 3 with those of laminar flow in a square duct in which Re=2000 and Pr=0.71. By making use of the fully developed, square-duct Nusselt number of 3.6, the corresponding Stanton number follows as 0.0025. As expected from the discussion in the penultimate paragraph, this value is considerably lower than the fully developed values indicated at the right-hand margin of Fig. 3. The other trends in Fig. 3 are similar to those already discussed in connection with Fig. 2.

Quantitative Pressure Drop Results. The pressure drop results will be presented from two points of view. One of these will display the actual streamwise pressure variations, and the other will be focused on friction factors. Figures 4 and 5 have been prepared to display the pressure variations as a function of streamwise position in the array.

The effect of Reynolds number on the streamwise pressure variation is exhibited in Fig. 4. The most noteworthy characteristic displayed in the figure is the periodic nature of the pressure distribution. This behavior is most strongly in evidence for Re_{hi}. In assessing the more evident periodic nature of the pressure variation for Re_{hi} relative to that for Re_{lo}, it is relevant to take account of the two contributions that give rise to pressure drop. For a

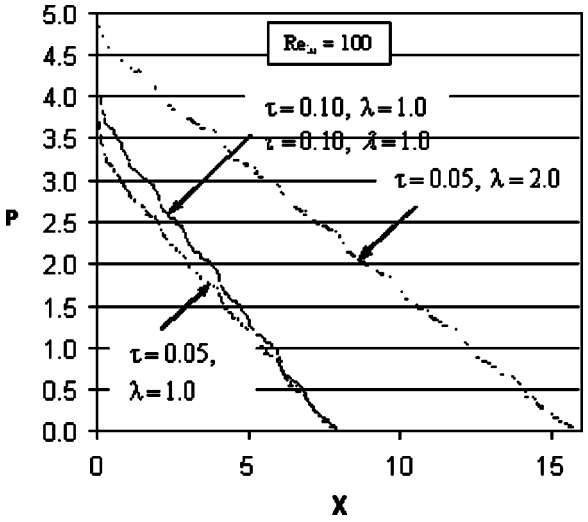

Fig. 5 Variation of the dimensionless pressure with streamwise position along the midplane of the array, $Re_{lo}=100$

low-Reynolds-number flow, the major contributor to pressure drop is fluid-surface viscous interaction while separation-related pressure drops are minimal. On the other hand, at high Reynolds numbers, both of these mechanisms are major contributors. Downstream of separated regions, there is a region of pressure recovery. Such pressure recovery is in evidence for the Re_{hi} case appearing in Fig. 4. On the other hand, in the absence of separated regions, there is no recovery mechanism, and friction causes a continuous decrease of the pressure.

The next figure showing pressure distributions is concerned with the effect of various geometric parameters for a fixed value of $Re_{lo}=100$. This information is conveyed by Fig. 5. The figure contains three curves, each of which corresponds to a particular geometry. Since all of the results exhibited in the figure correspond to Re_{lo}, there is little evidence of the pressure recovery that has already been discussed in connection with Fig. 4. Further inspection of Fig. 5 reveals that the effect of fin thickness is moderate, with only a slightly higher pressure drop for the dimensionless fin thickness $\tau=0.10$ compared with that for $\tau=0.05$. The $\lambda=2.0$ case corresponds to a fin which is of double streamwise length relative to the $\lambda=1.0$ case. For the former, the pressure drop per fin is larger, but not twice as large as the pressure drop per fin for the latter. On the other hand, the pressure drop per unit length of the array is smaller for the $\lambda=2.0$ case.

An alternative characterization of the pressure drop results can be made via the well-known friction factor. The friction factor is defined in what appears to be the conventional manner as

$$f=\frac{(-dp/dx)\omega}{(1/2)\rho\overline{U}^2}=2\frac{dP}{dX} \tag{28}$$

However, the evaluation of dP/dX has to be carried out keeping in mind the geometric periodicity. With this in mind, geometrically identical points separated by a streamwise distance L were selected and the pressures at these points were differenced, thereby providing the numerical value of dP/dX. This operation was performed for a succession of points in the streamwise direction, and the corresponding friction factors were evaluated.

Tabulation of the Quantitative Results. A listing of the fully developed Stanton numbers and friction factors is made in Table 2. The table is laid out with the case number on the left-hand margin and the adjacent St and f columns representing the results of the numerical simulations. Some of the Stanton numbers appearing in the table have already been exhibited in Figs. 2 and 3 along the right-hand margins. The friction factor listing in the table conveys new results. To provide perspective for the friction factor results, it may be noted that the friction factor for fully developed, laminar flow in a square duct is given by $f=57/\mathrm{Re}$. For Re=100, this gives $f=0.57$. This numerical value may be compared to the f values for cases 1, 3, . . . ,15 that appear in Table 2. It is interesting to observe that for those tabulated cases corresponding to long fins, the agreement between the fully developed duct flow and the offset fin array is quite satisfactory. On the other hand, for those cases characterized by shorter fins, the tabulated friction factors are substantially larger than 0.57. This behavior reflects the more frequent re-initiation of the boundary layer when the fins are short. A similar discussion may be made for the results of the higher Reynolds numbers.

Stanton Number—Friction Factor Correlation. Over the years, there have been many attempts to correlate heat transfer and friction results with a view to diminishing the need to separately measure these two quantities. The earliest work produced the well-known Reynolds Analogy ($f/2=\mathrm{St}$). This relationship was limited to fluids whose Prandtl number is approximately 1.0. Colburn [13] is credited with generalizing the Reynolds Analogy to make it applicable to fluids having Prandtl numbers different from 1.0, with the result $f/2=\mathrm{St}\,\mathrm{Pr}^{2/3}$. The latter is often referred to as the Colburn Analogy.

PROOF COPY 007406JHR

Table 2 Tabulation of fully developed St and *f* values

Case	St	f	Colburn Factor	Predicted St (32)	Predicted St (33)	Predicted St (34)	Predicted *f* (35)	Predicted *f* (36)	Predicted *f* (37)
1	0.096	0.86	5.63	0.098	0.098	0.096	0.92	0.92	0.86
2	0.0078	0.080	6.44	0.0078	0.0078	0.0077	0.086	0.088	0.080
3	0.097	0.86	5.57	0.098	0.098	0.096	0.92	0.92	0.86
4	0.0070	0.080	7.18	0.0078	0.0078	0.0077	0.086	0.088	0.080
5	0.10	0.98	6.16	0.098	0.098	0.10	0.92	0.92	0.98
6	0.0084	0.094	7.03	0.0078	0.0078	0.0079	0.086	0.088	0.094
7	0.10	0.98	6.16	0.098	0.098	0.10	0.92	0.92	0.98
8	0.0080	0.094	7.38	0.0078	0.0078	0.0079	0.086	0.088	0.094
9	0.085	0.58	4.29	0.087	0.087	0.085	0.63	0.64	0.58
10	0.0060	0.052	5.45	0.0056	0.0057	0.0056	0.057	0.058	0.052
11	0.085	0.58	4.29	0.087	0.087	0.085	0.63	0.64	0.58
12	0.0057	0.052	5.73	0.0056	0.0057	0.0056	0.057	0.058	0.052
13	0.088	0.68	4.86	0.087	0.087	0.089	0.63	0.64	0.68
14	0.0050	0.064	8.04	0.0056	0.0057	0.0058	0.057	0.058	0.064
15	0.091	0.68	4.70	0.087	0.087	0.089	0.63	0.64	0.68
16	0.0060	0.064	6.70	0.0056	0.0057	0.0058	0.057	0.058	0.064

The present results for St and *f* will be examined with regard to their adherence to the Colburn Analogy. For this purpose, it is convenient to define

$$\text{Colburn Factor} = (f/2)/(\text{St}\cdot\text{Pr}^{2/3}) \tag{29}$$

The Colburn factor was evaluated for the friction factors and Stanton numbers that were determined from the numerical simulations, and these values are listed in Table 2. The table reveals that the Colburn factor for the present results is well above 1.0, thereby indicating that the friction factor is notably larger than the Stanton number for the investigated geometries. This finding may be regarded as a failure of the Colburn Analogy. On the other hand, the analogy was developed for simple flows where flow separation is non-existent. Notwithstanding this, by selecting a representative value of the Colburn factor (for example, 6), it is possible to estimate a value of the friction factor provided the Stanton number is known, or vice versa.

Correlation of the St and *f* Using the DOS Method. From the statistical theory that underlies the DOS method, it is straightforward to develop correlations of the form

$$\text{St} = a_0 + a_1 A + a_2 B \ldots + b_1 AB + b_2 AC \ldots \tag{30}$$

where a_i are numerical coefficients and A, B, ... represent the independent parameters. A similar form can be used for the friction factor. Alternatively, a curve fit of the form

$$1/\text{St} = c_0 + c_1 A + c_2 B \ldots + d_1 AB + d_2 AC \ldots \tag{31}$$

can be constructed, and similarly for the friction factor. Support for the latter form can be obtained by observing that the Stanton number and the friction factor vary inversely with the Reynolds number and the fin length, both of which appear on the right-hand side of Eq. (31).

In the software that is used to process the DOS method, there is a focus on the relative importance of the various parameters with regard to their influence on the results. From the numerical information provided by this portion of the software, it was found that two of the four parameters, conductivity ratio and the dimensionless fin thickness had virtually no effect on the results. This is a major finding. On the other hand, the Reynolds number exerted a major influence upon the results, with the dimensionless fin length being of lesser importance.

In order to explore the sensitivity of the Stanton numbers predicted by the DOS correlation equations, several forms of the correlations were examined. These are

$$1/\text{St} = 5.131 + 0.03762\,\text{Re} - 1.191\lambda + 0.02480(\text{Re}\cdot\lambda) \tag{32}$$

$$\text{St} = 0.1144 - 5.228\times10^{-5}\,\text{Re} - 0.01147\lambda + 4.671\times10^{-6}(\text{Re}\cdot\lambda) \tag{33}$$

$$\text{St} = 0.1082 - 4.930\times10^{-5}\,\text{Re} + 0.0840\tau - 0.01147\lambda - 3.974\times10^{-5}(\text{Re}\cdot\tau) + 4.671\times10^{-6}(\text{Re}\cdot\lambda) \tag{34}$$

A comparison of the values of the Stanton numbers obtained from evaluating Eqs. (32)–(34) with the results directly obtained from the simulations is presented in Table 2. A careful inspection of the table indicates that for the majority of the cases (10 of the 16 cases) the agreement between the predictions of the fitted equations and the directly computed results is excellent, within a few percent. For the other cases, the deviations are generally within 10 percent. This level of agreement is regarded as a triumph of the DOS method in that it is able to provide excellent predictions based on a remarkably small number of direct simulations. A deeper examination of the table suggests that there is not a great difference in the accuracy of the different algebraic fits; however, strictly speaking, the best fit is provided by Eq. (34).

The friction factor results were also post-processed by the DOS method, yielding algebraic correlations. The correlation equations contain different numbers of terms in accordance with a consideration of the importance of the various parameters.

$$1/f = 0.3161 + 2.70\times10^{-3}\,\text{Re} + 0.224\lambda + 2.817\times10^{-3}(\text{Re}\,\lambda) \tag{35}$$

$$f = 1.268 - 5.758\times10^{-4}\,\text{Re} - 0.3037\lambda + 1.374\times10^{-4}(\text{Re}\,\lambda) \tag{36}$$

$$f = 1.095 - 4.992\times10^{-4}\,\text{Re} + 2.302\tau - 0.3037\lambda - 1.021\times10^{-3}(\text{Re}\,\tau) + 1.374\times10^{-4}(\text{Re}\,\lambda) \tag{37}$$

A test of the accuracy of these equations is set forth in Table 2. The table shows that there is a considerable difference in the efficacy of the various fitted equations. In particular, Eq. (37) provides a perfect representation of the results obtained from the direct numerical simulations, whereas the other two representations are of lesser accuracy. It is, therefore, recommended that Eq. (37) be used for any further predictions of the friction factor.

Qualitative Depiction of the Velocity Field. To illustrate the attainment of the periodic, fully developed flow field, a computed-generated contour diagram is presented in Fig. 6 for $\text{Re}_{lo} = 100$. The figure includes eight offset-fin modules. The velocity magnitude is represented by the various shades of gray which are keyed to the scale beneath the contour diagram. Careful study reveals that the attainment of the periodically fully developed regime is achieved after the second module. This rapid development is related to the low Reynolds number of the flow. At higher Reynolds numbers, the development length is somewhat larger.

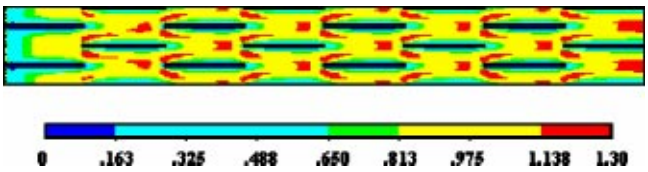

Fig. 6 Illustration of the velocity field corresponding to Re_{lo} = 100. The attainment of the periodic regime occurs after the second module.

Concluding Remarks

The practical problem of fluid flow and heat transfer in an offset-fin array which comprises the internal geometry of a cold plate has been solved by making use of direct numerical simulation in conjunction with methods of parameter minimization. The parameter minimization was accomplished by the use of two techniques. One of these makes use of nondimensionalized variables and parameters. Critical to this approach is the proper treatment of the boundary conditions. Once the reduction of the parameters had been accomplished, a second method, Design of Simulations (DOS), was employed to minimize the number of inputs needed to obtain an accurate representation of the parameter space. Although the original problem definition encompassed 11 parameters, only 16 simulation runs were required to provide the required information. Furthermore, the DOS method furnished algebraic correlations of the results obtained from the direct simulations so that the entire parameter space was fully covered. Another dividend of the DOS method was the identification of the importance of the various geometric and operating parameters.

The entire slate of results included Stanton numbers (dimensionless heat transfer coefficients), friction factors, and the development length for periodic and fully developed flow and heat transfer. The results enabled an assessment of the analogy between heat transfer and friction as embodied in the Colburn Analogy. This examination demonstrated that the complexity of the flow field gave rise to considerably larger friction factors than would have been predicted by the Analogy.

The algebraic format, Eqs. (32)–(37), facilitates various types of optimization studies. For instance, an algebraic form may be found for the pumping power as a function of the operating parameters of the problem. Such an algebraic representation would facilitate the use of a criterion such as constant pumping power.

Acknowledgments

The authors acknowledge with appreciation, the advice of Professor Perry Parendo of the University of St. Thomas concerning the DOS method. The support of H. Birali Runesha of the Supercomputing Institute for Digital Simulation & Advanced Computation at the University of Minnesota is gratefully acknowledged.

Nomenclature

c_p = specific heat of fluid
$\underline{f}$ = friction factor
h = per-module heat transfer coefficient
k = thermal conductivity
n = dimensional coordinate normal to a surface
N = dimensionless coordinate normal to solid-fluid interface, $=n/\omega$
p = pressure
P = nondimensional pressure, $=p/\rho\overline{U}^2$
Pe = Peclet number, $=\rho c_P \omega \overline{U}/k_{\text{fluid}} = \text{Re}\cdot\text{Pr}$
Pr = Prandtl number, $=c_P\mu/k_{\text{fluid}}$
Re = Reynolds number, $=\rho\omega\overline{U}/\mu$
q_{surf} = surface heat flux
St = per-module Stanton number, $=\overline{h}/(\rho c_p \overline{U})$
t = temperature
t_0 = fluid inlet temperature
T, L, H = fin thickness, fin length, and fin height
u, v, w = velocity components in the x, y, and z-directions
U, V, W = nondimensional velocity components in the x, y, and z-directions, $=u/\overline{U},\ v/\overline{U},\ w/\overline{U}$
$\overline{U}$ = average velocity
x, y, z = dimensional coordinates
X, Y, Z = nondimensional coordinates, $=x/\omega,\ y/\omega,\ z/\omega$

Greek Symbols

ρ = density
Θ = nondimensional temperature, $=t-t_0/(q_{\text{surf}}\omega/k_{\text{fluid}})$
τ, λ, η = nondimensional fin thickness, fin length, and fin height, $(\tau=T/\omega,\ \lambda=L/\omega,\ \eta=H/\omega)$
μ = viscosity
ω = channel width

Superscripts

$'$ = nondimensional thermophysical properties

References

[1] Wieting, A., 1975, "Empirical Correlations for Heat Transfer and Flow Friction Characteristics of Rectangular Offset Fin Heat Exchangers," ASME J. Heat Transfer, **97**, pp. 488–490.
[2] Kays, W. M., and London, A. L., 1984, *Compact Heat Exchangers*, 3rd ed., McGraw-Hill, New York.
[3] Hatada, T., and Senshu, T., 1984, "Experimental Study on Heat Transfer Characteristics of Convex Louver Fins for Air Conditioning Heat Exchangers," ASME Paper 84-HT-74.
[4] Joshi, H. M., and Webb, R. L., 1987, "Prediction of Heat Transfer and Friction in the Offset Strip Fin Array," Int. J. Heat Mass Transfer, **30**, pp. 69–84.
[5] Kurosaki, T., Kashiwagi, T., Kobayashi, T., Uzuhashi, H., and Tang, S.-C., 1988, "Experimental Study on Heat Transfer From Parallel Louvered Fins by Laser Holographic Interferometry," Exp. Therm. Fluid Sci., **1**, pp. 59–67.
[6] Manglik, R. M., and Bergles, A. E., 1990, "The Thermal-Hydraulic Design of the Rectangular Offset-Strip-Fin Compact Heat Exchanger," in *Compact Heat Exchangers*, R. K. Shah, A. D. Kraus, and D. Metzger, eds., Hemisphere Publishing Corp., Washington, D.C., pp. 123–150.
[7] Usami, H., 1991, "Pressure Drop Characteristics of Offset Strip Fin Surfaces," *Proceedings of the 1991 ASME/JSME Joint Thermal Engineering Conference*, **4**, J. R. Lloyd and Y. Kurosaki, eds., ASME, New York, pp. 425–432.
[8] Majumdar, ■. et al., 1992, "Heat and Momentum Transport in Oscillatory Viscous Flows," ASME J. Heat Transfer, **114**, pp. 866–875.
[9] Majumdar, ■. et al., 1997, "Oscillatory Momentum Transport Mechanisms in a Transitional Complex Geometry Flow," ASME J. Fluids Eng., **119**, pp. 29–35.
[10] Amon, ■. et al., 1992, "Numerical and Experimental Studies of Self-Sustained Oscillatory Flows in Communicating Channels," Int. J. Heat Mass Transfer, **35**, pp. 3115–3129.
[11] Montgomery, D. C., 2000, *Design and Analysis of Experiments*, 5th ed., John Wiley & Sons, New York.
[12] Patankar, S. V., Sparrow, E. M., and Liu, C. H., 1977, "Fully Developed Flow and Heat Transfer in Ducts Having Streamwise-Periodic Variations of Cross-Sectional Area," ASME J. Heat Transfer, **99**, pp. 180–186.
[13] Colburn, A. P., 1933, "A Method of Correlating Forced Convection Heat Transfer Data and a Comparison With Fluid Friction," Trans. AIChE **29**, pp. 174–210.